



**HAL**  
open science

# Classification of the Critical Resolved Shear Stress in the HCP materials by atomic simulation: Application to alpha-zirconium and alpha-titanium

A. Poty, J.-M. Raulot, H. Xu, David Rodney, C. Schuman, J.-S. Lecomte, C. Esling, M.-J. Philippe

## ► To cite this version:

A. Poty, J.-M. Raulot, H. Xu, David Rodney, C. Schuman, et al.. Classification of the Critical Resolved Shear Stress in the HCP materials by atomic simulation: Application to alpha-zirconium and alpha-titanium. *Journal of Applied Physics*, 2011, 110 (1), pp.014905. 10.1063/1.3599870 . hal-03864515

**HAL Id: hal-03864515**

**<https://cnrs.hal.science/hal-03864515>**

Submitted on 21 Nov 2022

**HAL** is a multi-disciplinary open access archive for the deposit and dissemination of scientific research documents, whether they are published or not. The documents may come from teaching and research institutions in France or abroad, or from public or private research centers.

L'archive ouverte pluridisciplinaire **HAL**, est destinée au dépôt et à la diffusion de documents scientifiques de niveau recherche, publiés ou non, émanant des établissements d'enseignement et de recherche français ou étrangers, des laboratoires publics ou privés.

# Classification of the Critical Resolved Shear Stress in the HCP materials by atomic simulation: Application to $\alpha$ -zirconium and $\alpha$ titanium

**Alexandre Poty<sup>1</sup>, Jean-Marc Raulot<sup>1,\*</sup>, Hong Xu<sup>2</sup>, David Rodney<sup>3</sup>, Christophe Schuman<sup>1</sup>, Jean-Sébastien Lecomte<sup>1</sup>, Claude Esling<sup>1</sup> and Marie - Jeanne Philippe<sup>1</sup>**

1) Laboratoire d'Étude des Microstructures et de Mécanique des Matériaux, LEM3, CNRS,

Université Paul Verlaine – Metz, Ile du Saulcy, 57045 Metz, France

2) Laboratoire de Physique des Milieux Denses (LPMD),

1 Boulevard Dominique François Arago, 57070 METZ Technopôle

3) Laboratoire SIMAP-GPM2

Domaine Universitaire BP 46, 38402 Saint Martin d'Herès, France

\*) corresponding auteur

## **Abstract**

The Embedded Atom Method (EAM) approach has been applied to the study of five principle gliding systems in zirconium and titanium materials. The stacking fault energy maps are obtained and compared to the results of ab initio calculations. A good agreement was observed between the two approaches. Furthermore, the Critical Resolved Shear Stresses (CRSS) have been determined by Molecular Dynamics (MD) simulations based on the EAM potentials. The CRSS in the “a” direction for the basal, prismatic (type 1) and pyramidal (type 2) planes are obtained and compared.

## **I. Introduction**

The zirconium (Zr) and titanium (Ti) are important materials for industrial applications. It is thus important to improve their properties and performance when subjected to extreme conditions of deformation (high strain rate and high speed or high temperature present in the forming process). Moreover, these materials are highly anisotropic, therefore it is important to control the relations between the deformation and the evolution of texture (or microstructure) in order to obtain the desired mechanical properties with the least energetic cost.

The majority of models predicting mechanical properties in deformed HCP materials are self-consistent models. They [1-2] are based on relationship between the experimental strain and stress ( $\sigma$ ,  $\epsilon$ ). They could provide simulated texture associated with desired mechanical properties [3]. However, these models require knowledge of systems strain, critical resolved shear stress (CRSS) and strain hardening induced among the most important gliding systems. During the last 20 years, mechanical behavior modelings of hexagonal materials try to obtain data of the CRSS and strain hardening matrices [1-3]. An important part of these CRSS data are unknown and are very different from one system to another. Consequently, one cannot simply apply the approach with only one isotropic strain hardening. In experimental conditions, the gliding systems are correlated. It is thus difficult to obtain the individual CRSS. And the atomistic simulation can be the ideal method to overcome this difficulty.

The adapted approaches to simulate the CRSS of dislocations with accuracy are ab initio or classical molecular dynamics (MD) methods. As dislocations are defects with long range interactions, the periodic boundary conditions of the ab initio program and the small simulation boxes used would create self-interaction between the dislocation and its periodic images. The ab initio approach is therefore only used to determine the stacking fault energies, which are related to the dislocation stability. On the other hand, the MD approach is used to calculate both the CRSS values and the stacking fault energies. We are thus able to compare the stacking fault energies obtained by the two approaches.

The key element for the accurate MD simulation is the interatomic potential. For the metals, the well adapted potential is the Embedded Atom Method (EAM) potential. Although most EAM potentials reproduce the equilibrium properties, some of them fail to describe correctly out-of-equilibrium conditions (movement of dislocations).

A recent EAM potential created by Mendeleev and Ackland [4] are fitted with the stacking fault energy obtained by many experimental and ab initio data for Zr. A comparison of this potential with the available others is made in this work. And for the Ti case, only the most used potentials are compared.

The paper is organized as following: in Section 2, we present the experimental method for measuring the CRSS of Zr. In Section 3, the ab initio and MD method are presented. In Section 4, the maps of stacking fault energy are shown and discussed. The best energetic paths are presented in Section 5 and the CRSS results are calculated in Section 6. And finally, we discuss the results and we conclude in Section 7.

## II. Experimental determination of the CRSS in the Zr monocrystals

### a) *Material and methods*

In the experiments, zirconium strips are used. The dimensions are 120 mm of length, 5 mm of wide and 1 mm of thick. The chemical composition of these strips is given in Table 1.

These strips were processed at 850 ° C for 5 days and then annealed at 700 ° C for 24 hours under high vacuum. This treatment allows the growth of the monocrystalline grains by the selection of variant during the recrystallization. After the treatment, the size of the grains reaches 15-40  $\mu$ m of diameter. These strips and heat treatments were performed by CEZUS compagny. Analysis of orientation with X ray diffraction and SEM technic have highlighted many homogeneous monocrystalline grain size requirements with very different directions. The grains selected for the determination of CRSS are those which under the effect of a uniaxial tension can activate only one principal system.

The micro tensile specimens are cut so that the single crystal studied corresponds to the useful area. After polishing, on the single crystal area, we introduced a microgrid with 0.5  $\mu$ m of square. The orientation of the single crystal surface has been previously determined. The tensile testing are done with the tensile machine directly in the SEM jed 845 in situ (Figure 1). Indeed, it is necessary to couple, during the test, both the mechanical response of sample (measure of the uniaxial stress and strain obtained by classical extensometer with the microgrids) and the observation of the emergence of corresponding mechanisms (monitored through optical imaging systems and electronic EBSD). The study of microgrids allows to verify the longitudinal and transverse homogeneity of the deformation in the areas where the first deformations appear. The activated deformation mechanisms will then be confirmed by transmission electron microscopy (TEM) post-mortem analysis.

### b) *Characterization of activated mechanisms*

If we know the evolution of the crystal orientation of grains during the test, it is possible to identify their mechanisms of formation. In principle, there are an infinite number of crystallographic planes giving a single mark on a surface of the specimen. However, if we limit ourselves to families of planes corresponding to the mechanisms usually taken into account in hexagonal materials (Table 2), it appears that we can remove some ambiguities. Furthermore, the post-mortem TEM checks confirm the activated systems (Figure 2).

### *c) Results*

By monitoring both stress strain curves during tensile test and the knowledge of the crystal orientation when the system is activated, it is then possible to determine the CRSS in this system. For these samples, we stayed at the step 1 (step where just one system is activated) of deformation which corresponds to 2% of strain. In this domain, one gliding system was highlighted. Three specimens for each system were used. The TEM observations are used to verify these mechanisms. Figure 2 shows stacks of type  $\langle a \rangle$  screw dislocation. The analysis shows that the grid deformation is almost homogeneous throughout the sample (at 2% strain). We were able to determine the shear stresses for prismatic and pyramidal glide  $\langle a \rangle$  respectively. For  $\langle c+a \rangle$  pyramidal glide, twinning has disturbed the test and the determined value is minimal because at this moment the glide was not continuously present in the specimen. The values obtained of the CRSS in the prismatic and pyramidal glide  $\langle a \rangle$  systems are respectively 35 and 40 MPa (Figure 3) and 55 and 60 MPa. The value of  $\langle c+a \rangle$  pyramidal system is between 90 and 110 MPa.

## **III. Simulation methods**

### *a) Ab initio*

The *ab initio* calculations have been performed based on the density functional theory (DFT)[5-7], using Vienna *ab initio* software package (VASP)[8-10]. The interaction between ions and electrons is described by ultra-soft pseudopotentials (USPP)[11]. The generalized gradient approximation (GGA) in Perdew and Wang parametrization[12-13] is used to describe the exchange-correlation energy and it is the best approach to describe magnetic materials. For the pseudopotentials used, the electronic configurations are for Ti ( $3d^34s^1$ ) and for Zr ( $4d^35s^1$ ). In this work, the kinetic energy cutoff is 300eV. For the unit cell, tests were carried out using different k-point meshes to ensure the absolute convergence of the total energy within a precision better than  $10^{-3}$  eV/atom. The best choice of Monkhorst-Pack[14] grid is to employ a  $8 \times 5 \times 5$  k-points grid within a unit cell. The density of k points in the unit cell is converged in the supercells and the kinetic energy cutoff is not changed.

All structures have been relaxed using the conjugate gradient algorithm and both the atomic position and volume have been optimized. We have used the unit cell to calculate the structural properties (a and c parameters and the cohesive energy). The stacking fault energy and the interface energies are obtained using supercells. These cells are the multiple of the unit cell with two motifs. A study of the convergence according to the distance between the

interfaces was realized and showed us that with a distance superior to 15Å, the energy of interface evolution is less than 0.2 mJ/m<sup>2</sup>.

For the maps of energy of interface, we used a sampling of 25×40 for the basal and type 1 prismatic plans and a sampling of 36×34 for the type 2 prismatic plan for both zirconium and titanium systems.

### ***b) Molecular dynamics (MD)***

We have used a laboratory code. The volume, the temperature and the number of atoms are fixed (NVT ensemble). The simulations are performed at the temperature 0K. The Newtonian equations of motion are integrated using a fifth-order Gear predictor-corrector algorithm. The Lagrange polynomial is used to fit a tabulated interatomic potential table. For each calculation, the relaxed structures are obtained by minimization of the energy. The convergence of the energy was reached and error on the energy is less than 0.0001 eV. The employed potentials in this work were based on the Embedded Atom Method (EAM)[15]. With this code, we have investigated the structural and elastic properties (a and c parameters, elastic constants, stacking fault energies) and the interface energies map.

The stacking fault energy maps are calculated with box of 8000 atoms. The box is divided in 2 smaller boxes. One box is fixed and the second box is moved in a two-dimensional space. The relaxations of each atom are permitted only in the third direction by MD quenching method.

Concerning the calculation to determine the critical stress results are obtained by ADD code built by D. Rodney[16-19] because it is very efficient to study a plastic deformations. We used the displacement of an edge dislocation which has been developed by the Osetsky and Bacon[20-21]. A simulation box is created with two half-crystals. The dimension of the two boxes are respectively N\*b and (N-1)\*b in the x direction, where N is an integer and b is the Burger's vector. The box is relaxed and the dislocation appears after relaxation to minimize the potential energy by MD quenching method.

### ***c) Interatomic potentials and crystal properties***

The HCP structure is not an easy structure to simulate at the atomic scale with the molecular dynamic (MD) method because of its anisotropy. Only few EAM potentials can predict correctly the essential structural, elastic and plastic properties. For example the reproducibility of the stacking fault energy (modeling parameter for the dislocation) is only obtained with a very recent Embedded Atom Method (EAM) potential[4]. Mendeleev and Ackland have used an approach based on the stacking fault energy obtained by many experimental and ab initio data

for Zr to fit EAM potentials. The values of the stacking fault energy presented in [4] are in agreement with the prism plane fault that has a lower value than that of the I2 basal plane fault. In Table 2, the 5 plans of gliding for HCP are shown (Table 2 and Figure 4).

To validate the EAM potentials for our study, we first performed tests consisting of calculations of the basic crystal properties. Concerning the study of the zirconium, we have tested several EAM potentials [4;22-28], in particular the two potentials built by Mendeleev et al.[4] and Ackland et al.[22]. As Khater et al.[29] we can observe several slight differences between the performance of these potentials. The results are presented in Table 3. We can see a good agreement between the experimental or *ab initio* values and our values while using the potentials on the structural properties. Concerning the elastic properties, the agreement is sometimes less good but remains acceptable.

In the study of the titanium material, we have considered essentially 2 EAM potentials, one by Pasianot[28], and one by Ackland[30]. We can observe a good agreement between the results obtained by *ab initio* calculation or/and the experimental data with the values of the semi-empirical EAM potentials (Table 4). Particularly, the Pasianot potential gives the best results.

#### *d) Stacking faults*

It is not only important that the potentials correctly reproduce the structural and elastic properties. To study the plastic properties associated with dislocations, it is also necessary to properly describe the energies of stacking faults. We investigated the energy of four different stacking faults (two intrinsic ones and two extrinsic ones).

The I1 stacking fault is created by the removing of a basal plane and a shift of half a crystal under the effect of minimizing the energy in the  $1/3$   $[10-10]$  direction (the ABABABABAB sequence becomes ABABBABAB then ABABCBCBC). The I2 stacking fault is created by the replacement of A planes by C planes and the B planes by A planes (we can imagine a displacement of half crystal in the  $1/3$   $[10-10]$  direction, the ABABABABAB sequence becoming ABABCACACA). The E extrinsic fault is obtained by inserting a C plane (the ABABABABAB sequence becomes ABABCABAB). Finally, the T2 stacking fault results, only, from a gliding of one A plane in the direction  $1/3$   $[10-10]$  giving one C plane (the ABABABABAB sequence becomes ABABCBAB).

We first calculated with the *ab initio* method, the energies of stacking faults for zirconium and titanium. Subsequently, we have calculated the same stacking faults with the semi empirical EAM potentials. There are different effects. Overall, the values obtained by *ab initio* method are larger than the values obtained with molecular dynamics. On the other hand, we find that

I2 and T2 stacking fault energies are very close when using the MD method, whereas with the ab initio method, the values are found quite different.

It appears clearly that the energies of stacking faults are underestimated with the EAM potentials. They thus cannot reproduce the subtle differences (small energetic variation between I2 and T2 stacking fault). However, we note that the Mendeleev potential for zirconium gives values in agreement with ab initio calculations. Concerning the titanium material, although the data obtained by ab initio and MD are different, we will still retain in rest of the article, the titanium potential by Pasianot, because its results are closer to ab initio ones than the other EAM potential tested (see Table 4). The resultants are in agreement with the literature [31-32]

#### **IV. Interface energies map**

After validation of the EAM potentials, we have studied the variation of the stacking fault energy ( $\gamma$ ) for 5 systems of gliding shown in Table 2. We have compared the results found with 2 methods (molecular dynamics (MD) and ab initio calculations). In both methods, the direct and the indirect ways are considered.

The  $\gamma$  energies consist of the difference between the energy of the out of not equilibrium system and the energy of the equilibrium system divided by the area of the surface. We plotted the data obtained by ab initio and molecular dynamics calculations for Zr and Ti. Super cells are constructed in order to avoid interaction between the interfaces. The techniques used are the following. Half of the supercell is moved in two dimension space, exploring the surface with a sampling corresponding to  $n_x \times n_y$  points. We used 25x40 points for basal and prismatic 1 planes, 36x34 for the prismatic 2 plane, 25x90 points for type 1 pyramidal plane and 44x47 points for type 2 pyramidal plane. Figures 5 to 9 show the results for Zr and Figures 10 to 14 show the results for Ti. The “a” figures illustrate the data obtained with the method of molecular dynamics and the “b” figures those obtained by ab initio calculations. Although the figures are qualitatively similar, there exist a few quantitative differences in shape, geometry and intensity.

##### ***a) Zr case***

In the case of Zr basal plane, there is a maximum between each atomic site and a relative minimum in the direction  $1/3[10-10]$  with the MD method (the 4 corners and the center of Fig.5a). Each site is enclosed in 3 regions with a maximum energy and 3 regions with a relative minimum energy. With the ab initio method, we observe the same geometry: 3 regions

with a maximum energy and 3 regions with a relative minimum energy on the basal plane (Figures 5c).

The  $\gamma$  energies of the type 1 prismatic plane obtained by MD and ab initio calculations are similar (Figures 6.a and 6.c). There is a small massif with low energies in the “a” direction and a big massif in the “c” direction with high energies. It is clear that the displacements in the “c” direction are subject to a component in “a” direction, because the best energetic way in the “c” direction is to pass by the center of the figure that is a saddle point. The sites of maximum energies are localized on the c-axis in MD method and they are slightly shifted out the c-axis with the ab initio approach.

The  $\gamma$  energies obtained for the type 2 prismatic planes with MD and ab initio approaches have the same symmetries but they are very different in magnitude (Figures 7.a and 7.c). There is a high energy peak in the [1-100] direction and a peak with low energy in the “c” direction. In this plane, the displacements in the c direction are subject to a shift in the [1-100] direction. As the type 1 prismatic plane the center of the figure is a saddle point and the best energetic way in the c direction is to pass by the center of the plane.

The calculation of the  $\gamma$  energies for the pyramidal planes necessitates the use of a very large supercell. Only results with MD method are displayed here, because the time cost for an ab initio calculation would be out of the reach at present. Concerning the type 1 of the pyramidal plane (Figure 8.a), we can observe a minimum of the energy on the map in each corner and at the center. The location of these minimums forms triangles. In the center of these triangles, there is a region where the  $\gamma$  energy is high (situated close to 1/4 of the c+a direction if the starting point is (0,0) or 3/4 of the c+a direction if the starting point is (0, 1/2)). We can see, in the “a” direction, that the  $\gamma$  energy is low and the energetic best way is not exactly the “a” direction but we must consider a small component in the “c+a” direction.

In the type 2 pyramidal plane (Figure 9.a), there is a big energetic massif in the middle of the [1-100] direction. This massif has a saddle point in the center of the map. We can observe that the “c+a” way is energetically favorable and there isn't other best way in this plane.

### ***b) Ti case***

Figures 10.a and 10.c represent the  $\gamma$  energies of Ti in the basal plane by MD and ab initio method. We observe the same behavior as for Zr: each site is enclosed by only three maximums (or three minimum) with MD approach and with ab initio method. The  $\gamma$  energy close to the equilibrium site has a triangular expected shape in the map obtained by ab initio

method in the titanium case. The maximum energies are lower than those observed in case of Zr with MD approach and it is the opposite with ab initio method.

The  $\gamma$  energies of type 1 prismatic planes obtained by MD and by ab initio methods are different (Figures 11.a and 11.c). There is a low energy massif in the “a” direction and there is a high energy massif in the “c” direction in both cases but the energetic maximums of the both massifs obtained by ab initio method are higher than the maximum obtained by the MD method. The two massifs at the middle in the “a” and “c” directions tend to be closer than the Zr case. It is expected because the lattice parameters of Ti are smaller than that of Zr. Concerning the displacement in the “c” direction, the most favorable energetic way passes by the middle of the map with MD method. This saddle point at the center of the map is not present in the ab initio results. In this case the best path, concerning the displacement in the c direction, is the direct way.

The  $\gamma$  energies of type 2 prismatic planes (Figures 12.a and 12.c) obtained by MD and ab initio approaches are quite different, although containing some similar aspects. In MD method, there is a high energy peak in the [1-100] and a peak much lower in the “c” direction as in the zirconium case. A path of least energy passing through the center of the map can be followed by the atoms. The symmetry around the site of equilibrium has a square shape.

In the ab initio results (Fig.12.c), we see that the peaks in the middle of directions [1-100] and [0001] are the higher than MD results. The symmetry around the site has an equilibrium form of diamond.

The type 1 of pyramidal  $\gamma$  energy plane is presented in Figure 13.a, we can observe a minimum of the energy on the map in each corner and at the center. The shape of these minimums is not perfectly spherical. Between these minimums in the  $\langle 11-23 \rangle$  direction, there are maximums of energy. These maximums create large region with small connections in the  $\langle 11-20 \rangle$  direction. The symmetry of the maximum or minimum energies lattice is the same. The distance between two extrema is  $\frac{1}{2} \langle 22-43 \rangle$ . It is clear, in the “a” direction, that the  $\gamma$  energy is low and the energetic best way is quasi the “a” direction but we must consider a small component in the “c+a” direction.

In the type 2 pyramidal plane (Figure 14.a), we can observe very little difference between the Zr case and the Ti case. There is a big energetic massif in the middle of the [1-100] direction. This massif has a saddle point in the center of the map. We can observe that the direct “c+a” way is energetically favorable and there isn't other best way in this plane.

## V. Best energetic ways

The maps of  $\gamma$  energies for Ti and Zr have similarities but also significant differences (maximum of energy, level of the saddle point). To better understand of the pathway followed by the atoms, we plotted a cut of the direct and the indirect energy paths (if the indirect paths exist) in “a” and “c” directions.

### *a) Zr case*

The energy paths obtained by MD and ab initio method, in the basal plane, are represented by Figures 5.b and 5.d. For direct paths, the difference between the two methods is 20% concerning the maximum of the energy in the direct “a” direction. In considering the curves of indirect paths, the gap increases slowly. The energy gain of the indirect path compared to the direct path is 36% for calculation of MD approach and 37 % for ab initio calculations.

In the type 1 prismatic plane (Figures 6.b and 6.d.), we observe that the way in the “a” direction is energetically the lowest. There is no indirect path in the “a” direction. The direct path in the “c” direction has a very high energy peak (1000 and 2000 mJ/m<sup>2</sup> for MD and ab initio methods, respectively). A more favorable energetic way passes by the center of the map in the both approaches. It is observed that the indirect path has two relative minimums and that the energy gain between the two paths is 27% and 43% for MD and ab initio methods, respectively. We can also see that the local minimums are more stable with the method of MD than the ab initio calculations (deeper valleys).

For the prismatic plane of type 2 (Figures 7.b and 7.d), we consider only the direct and indirect paths in the “c” direction. The indirect path passes close to the middle of the map where the energy is lower than the energy of the maximum (787 and 531 mJ/m<sup>2</sup> for MD and ab initio methods, respectively). The maximum energies are 934 and 1280mJ/m<sup>2</sup> for the indirect paths obtained by the MD and ab initio methods, respectively. The relative minimum is more stable with the ab initio method than that obtained with the MD approach. The energy difference between the two paths is therefore 38% and 46% for MD and ab initio methods, respectively. As the energetic wells of the relative minimums are deeper with the ab initio method, the relative minimum is more stable.

The energetic ways obtained with pyramidal map with MD method are presented at Figures 8.b and 8.b. Concerning the type 1 of the pyramidal plane (Figure 4.b) with the “a” direction, we can observe a direct way and an indirect way with a minimum of energy at the middle. The maximum with the direct and the indirect way are 441 and 405 mJ/m<sup>2</sup>, respectively. The

relative maximum difference between these two paths is 9%. In the “c+a” direction, we can observe on the direct way two peaks with different maximums of energy (2040 and 1750 mJ/m<sup>2</sup>). This effect shows energetic anisotropy depending on the direction of displacement. This effect disappears with the “c+a” indirect way. The “c+a” indirect passes by the center of the plan. The maximum of the energy obtained in the “c+a” indirect way is 1750 mJ/m<sup>2</sup>. In this case, the energy difference between the two paths is 17% and nearly 0% for the 2 peaks, respectively.

On the type 2 of pyramidal plane (Figure 9.b), we can see only the direct way. The maximum of the energy is 771 mJ/m<sup>2</sup> in the “c+a” direction. We can observe that the glide in the “c+a” direction on the (11-22) plane is easier than the glide on the (10-11) plane.

### ***b) Ti case***

The energy paths obtained by MD and ab initio calculations in the basal plane are represented by Figures 10.b and 10.d. There are similarities with the zirconium case. However, contrary to Zr, the energy values obtained by the MD approach are slightly lower than those obtained with the ab initio method. For direct paths, the difference between the two methods is of the order of 28%. In examining the curves of indirect paths, we notice that the gap increases (31%).

Similar to Zr, the energy gain of the indirect path compared to the direct path is 17% for MD calculation and 13% for the ab initio calculation. The “a” indirect path has a relative minimum at the middle of the way (285 and 416 mJ/m<sup>2</sup> for MD and ab initio methods, respectively).

Concerning the prismatic plane of type 1 (Figures 11.b and 11.d.), we observe that the path in the “a” direction is energetically the lowest, in Zr case. So there is no indirect path in this direction. The direct path in the “c” direction has a very high energy maximum (928 and 2030 mJ/m<sup>2</sup> for MD and ab initio methods, respectively). In the “c” direction and with the MD method only, there is a more favorable energy path passing by the center (713 mJ/m<sup>2</sup>). The relative minimums observed are shallow and the energy gain obtained between the two paths is 23%.

For the prismatic plane of type 2 (Figures 12.b and 12.d.), we consider only the direct and indirect paths in the “c” direction, as for Zr. The indirect path passes close to the middle of the map (883 mJ/m<sup>2</sup> for MD method and 1475 mJ/m<sup>2</sup> for the ab initio approach) where the energies are lower compared to the maximum energies. The maximum energy of indirect

paths are 1080 and 599 mJ/m<sup>2</sup> for MD and ab initio methods, respectively. The relative minimum is more stable with the ab initio method than that obtained with the approach of MD. The energy difference between the two paths is quite important, 38% and 42% for MD and ab initio methods, respectively. The relative minimum wells are deeper for the ab initio method, indicating that the relative minimum is more stable than the MD result.

As in Zr case, in the type 1 pyramidal plane (Figures 13.b and 13.d.), we observe that the way in the “a” direction is energetically the lowest. The direct way and the indirect paths in the “a” direction is energetically quasi equivalent. The maximum with the direct and the indirect way are 469 and 459 mJ/m<sup>2</sup>, respectively. The relative maximum difference between these two paths is 2%. In the “c+a” direction, we can observe on the direct way two peaks with different maximums of energy (1930 and 2130 mJ/m<sup>2</sup>). As in Zr case, this effect shows energetic anisotropy depending on the direction of displacement. This effect disappears in the “c+a” indirect way. The “c+a” indirect passes closed to the center of the plane. The maximum of the energy obtained in the “c+a” indirect way is 1930 mJ/m<sup>2</sup>. In this case, the energy difference between the two paths is 10%.

In the type 2 of pyramidal plane (figure 14.b), we can see only the direct way. The maximum of the energy is 932 mJ/m<sup>2</sup> in the “c+a” direction. We can observe that the glide in the “c+a” direction on the (11-22) plane is easier than the glide on the (10-11) plane.

To summarize, the paths of minimum  $\gamma$  energy for Ti and Zr are similar but they also show quantitative differences. For the basal plane, we observe the same behavior with the two materials. There is an indirect path through the direction  $1/3 [10-10]$ . This path reduces the energy barrier of 13-20%. The indirect path reveals a position energetically stable.

For prismatic planes, the differences between Ti and Zr are larger, because for Ti, the energies obtained by ab initio are twice the energies obtained by MD. In the case of prismatic plane of type 1 and for Ti, there is no indirect path resulting from a method for ab initio .

For the prismatic plane of type 2, the minimum energy of the indirect path obtained by the ab initio method is more stable for both Ti and Zr systems. It can be also noted that energy to travel through the path is more important for Ti case than for Zr case (this with both approaches, but the effect is stronger for the ab initio results).

In Figures 11 and 12, we summarize all the results of maximum energies obtained in this study, for Zr and Ti respectively.

## **VI. Critical Resolved Shear Stress (CRSS)**

In this part, we calculate directly the CRSS in the edge dislocation in the  $1/3[11-20]$  direction with 3 types of planes (basal, prismatic, and pyramidal planes).

The shear stress for edge dislocation is due to the inherent resistance of atoms in the crystal. In the absence of temperature effects ( $T = 0\text{K}$ ), the shear stress is equal to the Peierls stress. We have determined the Peierls stress in the basal, type 1 pyramidal and type 1 prismatic planes only in the “a” direction. In fact, the  $\gamma$  energy calculations show that this is the direction that has the lowest energy. We follow the protocol by Bacon[17-18], and the MD code is adapted from that of Rodney[] initially used for cubic materials. We fix a block composed several layers of atoms and we move a equivalent block to the opposite side to create a shear. The atoms between the two blocks are mobile and can relax. The core of the dislocation can then move freely under the effect of shear. The relative increment of displacement is  $10^{-5}$ .

Stress strain curves of crystals containing dislocations for the three slip systems are shown in Figure 15 for zirconium and Figure 16 for titanium. Concerning zirconium, the CRSS values have been calculated and are 3.5, 14 and 21 MPa for basal, pyramidal and prismatic planes respectively. If we normalize the CRSS values obtained by the lowest CRSS value, we find the following ratios: 1, 4.1 and 6.2. For titanium, the CRSS are 3.1, 4.2 and 12 MPa for the basal, pyramidal and prismatic planes respectively. After normalization, we obtain the following ratios: 1, 1.3 and 3.8. We can observe that both systems show the same ranking of CRSS ratios: the glide along the basal plane seeming to be the easiest, followed by the pyramidal plane of type 1, where the gliding is easier than the third system, with the prismatic plane of type 1. These results are quite different from the classifications obtained based the the  $\gamma$  energies for Zr and Ti (Figs 17-18).

## VII. Discussion and Conclusion

The hierarchy prediction of gliding systems in hexagonal materials has been investigated by many researchers[33]. Peierls was the first to suggest that the dislocations pass by energetic saddle points. These saddle points opposing movements of dislocations are considered as friction forces. Several more or less refined models were created for predicting the slip systems. Legrand [34-35] suggested a criterium with the parameter  $R = \frac{\gamma_{basal} C_{66}}{\gamma_{prism} C_{44}}$ . If  $R < 1$  the main glide is basal, if  $R > 1$ , the main glide is prismatic and if  $R \cong 1$  then both basal and prismatic glides can take place.  $\gamma_{basal}$  is the stacking fault energy in the basal plane and the  $\gamma_{prism}$  is the stacking fault energy in the prismatic plane.

In the present, for the case of zirconium, the energies of basal and prismatic stacking faults are respectively 199 mJ/m<sup>2</sup> and 145 mJ/m<sup>2</sup> by MD and 213 mJ/m<sup>2</sup> and 166 mJ/m<sup>2</sup> by ab initio method. Although, the values of elastic constants of potential Mendeleev and experimental values are close, the  $C_{66}/C_{44}$  ratio is estimated 0.88 by MD while the ratio obtained by ab initio is 1.13. On the other hand, from the section 4, the values of  $\gamma$  energy in the basal and prismatic planes obtained with the MD method and the ab initio method are in good agreement.

The R ratio obtained by Legrand for Zr case was 2.3[34]. That obtained by the present MD investigation is 1.20 and we obtain 1.44 by ab initio approach. As these R ratio are higher than 1 and that the gliding should be the prismatic of type 1 glide. Nevertheless, the order of CRSS obtained in the section 6 predicts that the glide in the basal plan is the primary system.

For Ti case, we obtained R ratios of the same order of magnitude. The energies of basal and prismatic stacking faults are respectively 246 mJ/m<sup>2</sup> and 217 mJ/m<sup>2</sup> by MD and 336 mJ/m<sup>2</sup> and 206 mJ/m<sup>2</sup> by ab initio method. The  $C_{66}/C_{44}$  ratio obtained is 1.15 by MD while the ratio obtained by ab initio method is 1.04 [36].

The Ti R ratio obtained by Legrand was 2.6 and that obtained by MD and ab initio methods are respectively 1.30 and 1.70. As in Zr case, although the glide should be the primary prismatic slip, the order of CRSS obtained in the section 6 gives that the basal glide as the principle gliding system.

We have calculated the  $\gamma$  energy for 5 planes of glide to the zirconium and titanium by MD and ab initio methods, complementing previous studies. The  $\gamma$  energies obtained with the two methods are in good agreement and are consistent with results from other research groups.

We plotted the paths of lower  $\gamma$  energy which could be followed by the atoms during the movement of dislocations in these HCP materials. These paths are in agreement with the experimentally observed paths and with instability of dislocations resulting in the creation of partial dislocations.

We have given a classification involving the  $\gamma$  energies of the saddle point (for the paths of least energy). This normalized classification predicts that the prismatic glide of type 1 in the  $\langle a \rangle$  direction is the easiest. These results are in agreement with the experimental results obtained for Zr.

The CRSS have been obtained for the two gliding systems for which the  $\gamma$  energies are the lowest. The results are in agreement with previous simulations[29] but they do not correspond to the order of the classification with  $\gamma$  energies and to the experimental results. Khater et al. [29], who studied the screw dislocations in Zr have not observed an hierarchy in agreement with experimental results either.

In conclusion, our results show that it is necessary to improve both the EAM potentials and the dislocation model, in order to better determine the CRSS in the hexagonal materials. For example the EAM potential for Ti should be able to tell the difference between I2 and T2 stacking faults. A dislocation model which is more complicated than that of [26] should be suggested, including equally the screw dislocation. In the new model, the presence of oxygen, which is included in the defects and which affects the CRSS, should be considered.

Table 1 chemical composition (weighted percent)

Zr	O <sub>2</sub>	Fe	Hf
Balance	400 to 500 ppm	20 ppm	50 ppm

Table 2 : Properties of the Zirconium obtained by *ab initio* and MD calculation with different EAM potentials.

Plan of glide		Direction of glide	
name	plan	direction	Burgers vector
Basal	(0001)	<11-20>	$\vec{a}$
Prismatic 1	(10-10)	<11-20>	$\vec{a}$
Pyramidal 1	(10-11)	<01-10>	$\vec{a}$
Pyramidal 1	(10-11)	<11-23>	$\overrightarrow{c + a}$
Pyramidal 2	(11-22)	<11-23>	$\overrightarrow{c + a}$
Prismatic 1	(10-10)	<0001>	$\vec{c}$
Prismatic 2	(11-20)	<0001>	$\vec{c}$

Table 3 : Properties of the Zirconium obtained by *ab initio* and MD calculation with different EAM potentials.

Properties	th	Ex[31]	Ackl[25]	Ackl[22]	Mend2.[4]	Mend3[4]	Cler1[25]	Cler2[25]	Will[27]	Will[27]	Pasia[28]
a (Å)	3.208 7	3.230	3.266	3.249	3.220	3.232	3.152	3.233	3.226	3.164	3.232
c (Å)	5.139 3	5.150	5.212	5.183	5.215	5.172	5.137	5.254	5.257	5.156	5.149
c/a	1.602	1.594	1.595	1.619	1.619	1.600	1.630	1.625	1.630	1.630	1.593
Ec (eV)	(-8.5)	-6.32	-6.26	-6.25	-6.47	-6.64	-6.16	-6.03	-6.17	-6.52	-6.25
C <sub>11</sub> (GPa)		155.4	157.6	160.1	164.8	146.5	146.9	150.8	158	172.8	140.5
C <sub>12</sub> (GPa)		67.2	74.9	76.0	65.1	69.3	76.4	56.6	74.8	81.9	66.1
C <sub>13</sub> (GPa)		64.6	71.7	70.2	63.6	75.7	65.8	46.5	36.6	60.2	60.4
C <sub>33</sub> (GPa)		173.0	161.6	175.6	180.5	168.2	158.4	166.7	171.4	187.9	162.1
C <sub>55</sub> (GPa)		36.3		35.1		43.8					28.5
C <sub>66</sub> (GPa)		41.1	41.4	42.1	49.9	38.6	35.3	47.1	41.6	45.5	37.2
Ev (eV)		2.08	1.78	1.79	2.27	1.76	1.79	2.63	2.07	2.17	1.73
I1 (eV/Å <sup>2</sup> )	10.5		1.7	1.8	3.4	6.2	0.8	4.5	0.9	1.1	2.2
I2 (eV/Å <sup>2</sup> )	14.2		3.5	3.5	6.9	12.4	1.6	8.9	1.8	2.1	4.4
E (eV/Å <sup>2</sup> )	18.5		5.2	5.3	10.3	18.7	2.4	13.4	2.7	3.2	6.7
T2 (eV/Å <sup>2</sup> )	14.2		3.5	3.5	6.9	12.4	1.6	8.9	1.8	2.1	4.4

Table 4 : Properties of the Titanium obtained by *ab initio* and MD calculation with different EAM potentials.

Properties	ab initio	Exp[31]	Pasianot[28]	Ackland[30]
a (Å)	2.934	2.951	2.951	2.966
c (Å)	4.641	4.679	4.686	4.728
c/a	1.582	1.586	1.588	1.594
Ec (eV)	(-7.73)	-4.86	-4.85	-4.85
C <sub>11</sub> (GPa)		176.1	186.5	190.0
C <sub>12</sub> (GPa)		86.9	73.1	79.6
C <sub>13</sub> (GPa)		68.3	68.0	81.5
C <sub>33</sub> (GPa)		190.5	190.3	242.2
C <sub>55</sub> (GPa)		50.8	49.2	56.9
C <sub>66</sub> (GPa)		45.0	56.7	55.2
Ev (eV)			1.53	1.44
I1 (mj/m <sup>2</sup> )	9.7		3.6	2.2
I2 (mj/m <sup>2</sup> )	17.3		7.1	4.3
E (mj/m <sup>2</sup> )	24.4		10.7	6.5
T2 (mj/m <sup>2</sup> )	21.9		7.1	4.3

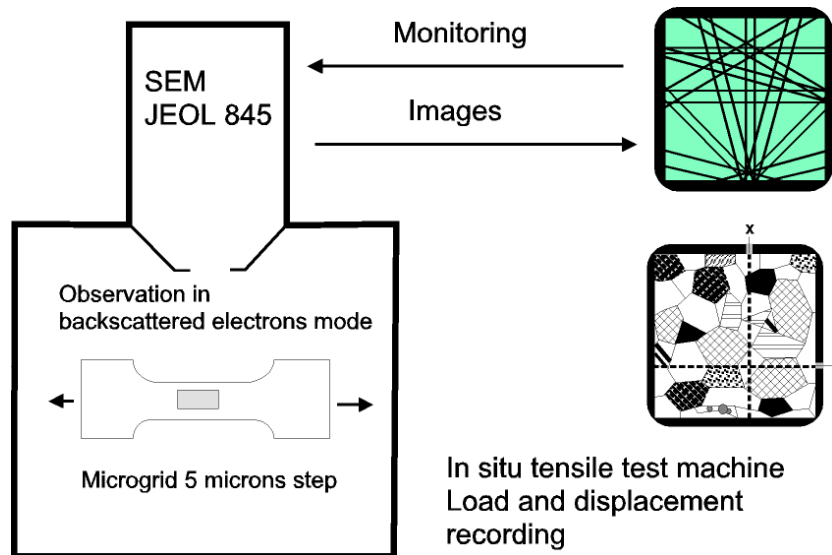


Figure 1 Block diagram of the equipment

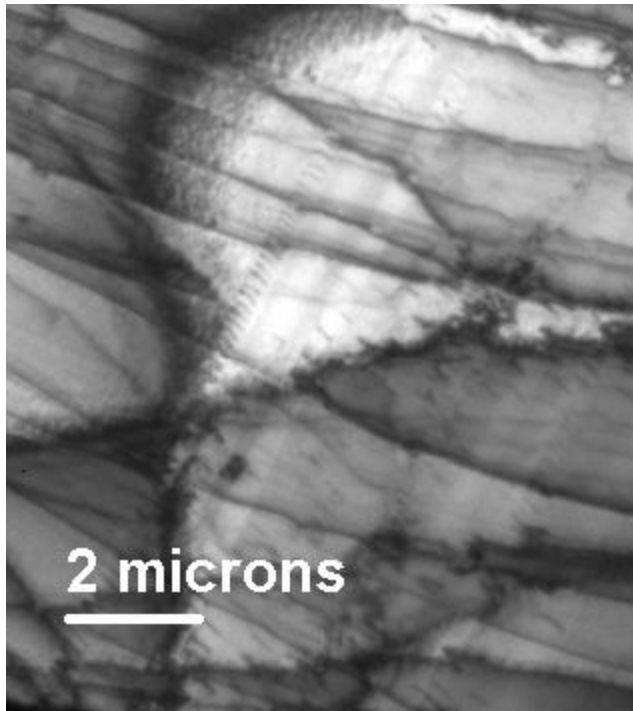


Figure 2 : the pile-ups of  $\langle a \rangle$  dislocations in prismatic plane observe by TEM.

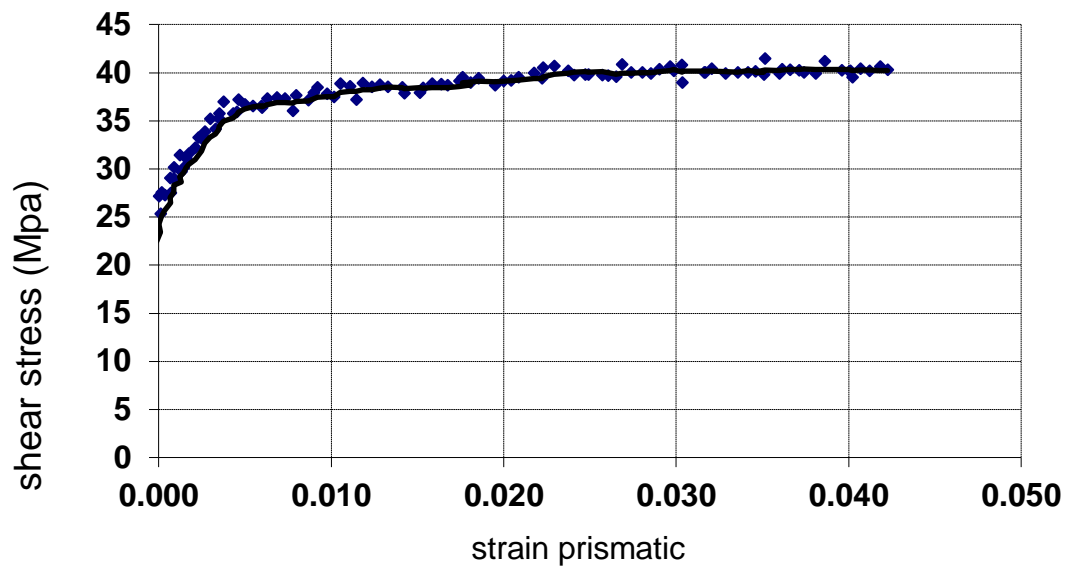


Fig 3 : Stress vs strain deformation of the prismatic gliding

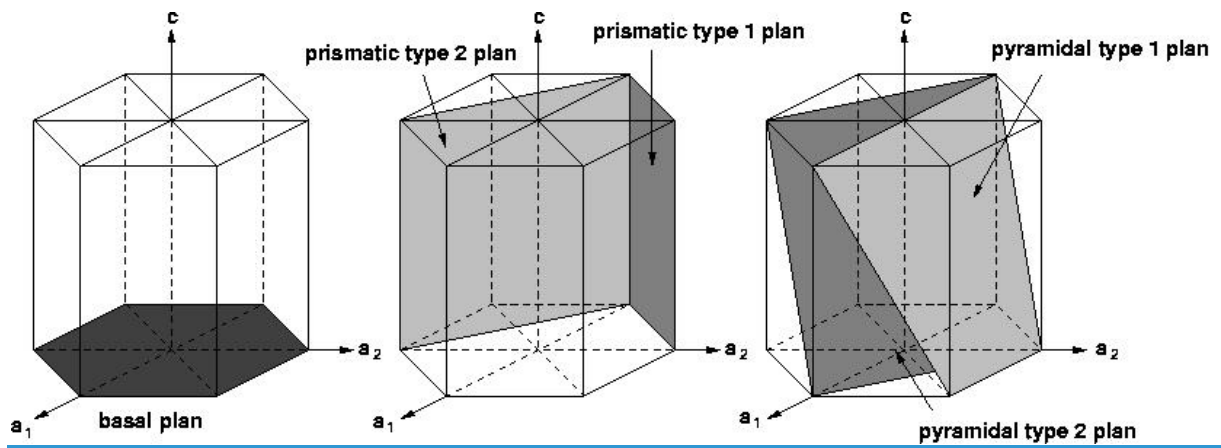


Figure 4: HCP cell with the different plans: the hcp cell is represented (at the left) with basal plan, (at the center) with the prismatic of type 1 and of type 2 plans, (at de right) with the pyramidal of type 1 and of type 2 plans.

Zr

Basal

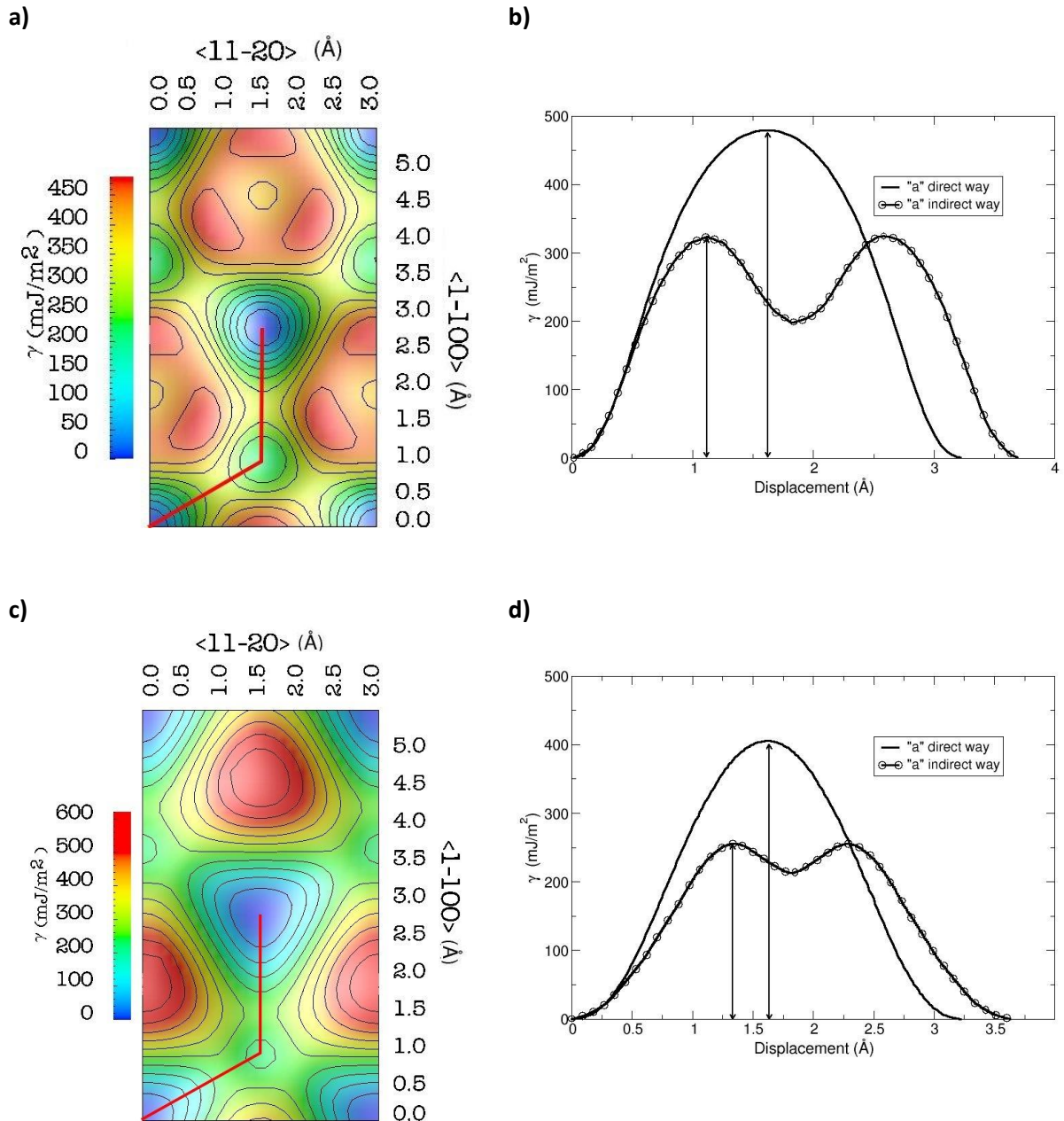


Figure 5: Zirconium. On the top left picture (a): Map of the stacking fault energy ( $\gamma$ ) in the (0001) plan obtained by MD. On the bottom left picture (c): Map of stacking fault energy ( $\gamma$ ) in the (0001) plan obtained by *ab initio*. On the top right (b): graphic of energetic way following the "a" direction obtained by MD. On the bottom right (d): graphic of energetic way following the "a" direction obtained by *ab initio*. The red lines represent the indirect paths.

Zr

Prismatique

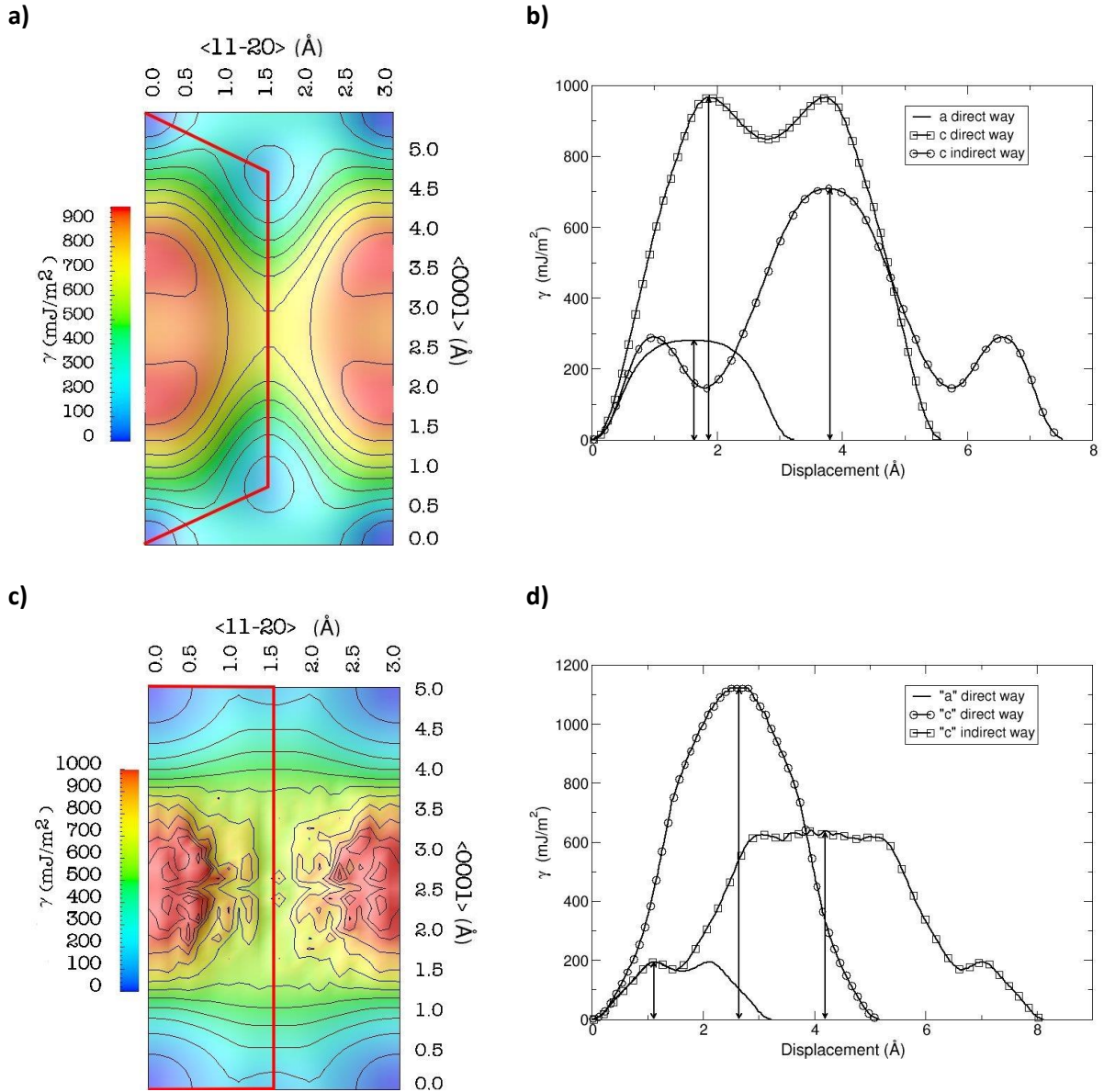


Figure 6: Zirconium. On the top left picture (a) : Map of the stacking fault energy ( $\gamma$ ) in the (10-10) plan obtained by MD. On the bottom left picture (c): Map of stacking fault energy ( $\gamma$ ) in the (10-10) plan obtained by *ab initio*. On the top right (b): graphic of energetic way following the “a” and “c” directions obtained by MD. On the bottom right (d): graphic of energetic way following the “a” and “c” directions obtained by *ab initio*. The red lines represent the indirect paths.

Zr

### Prismatique 2

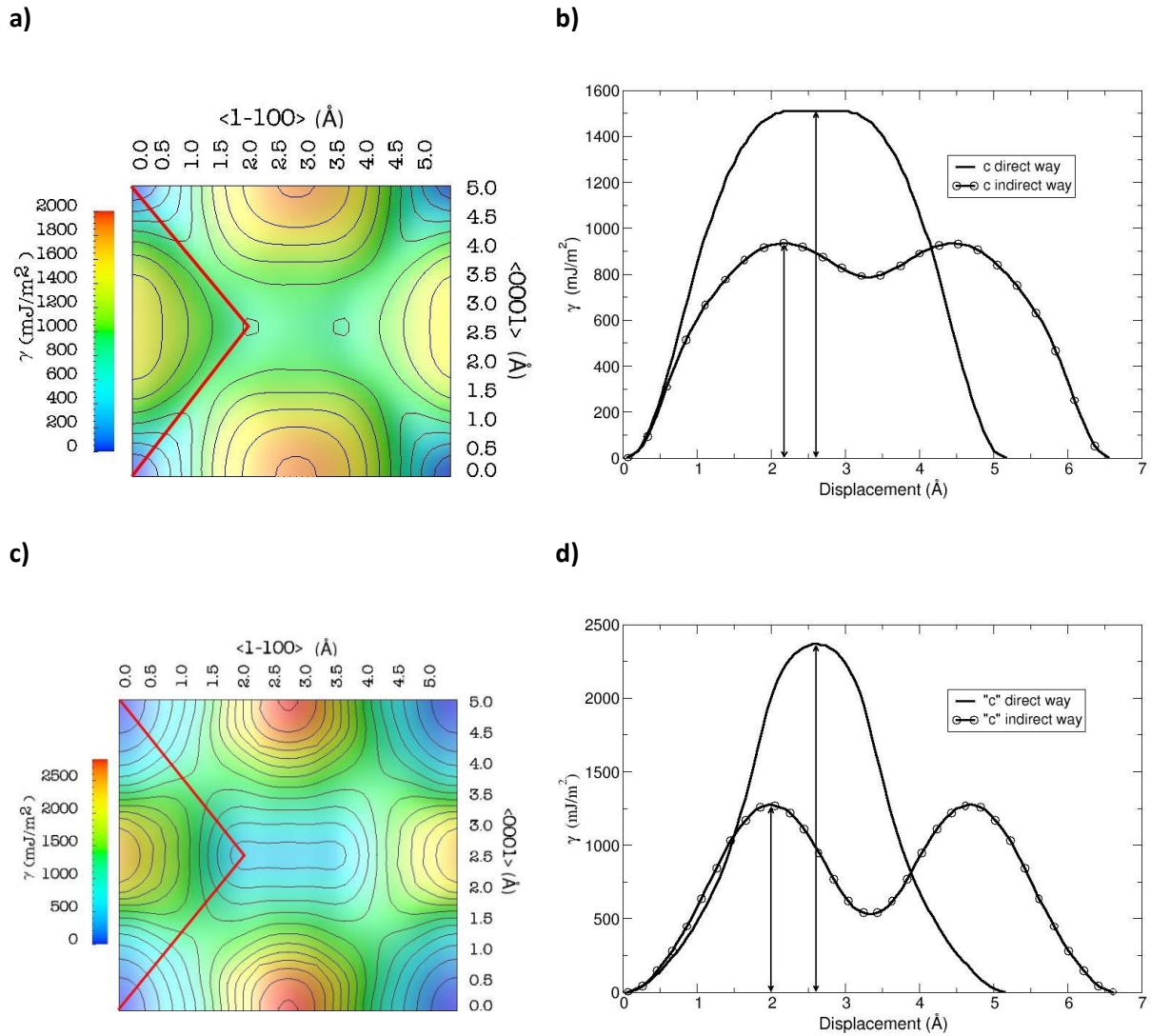
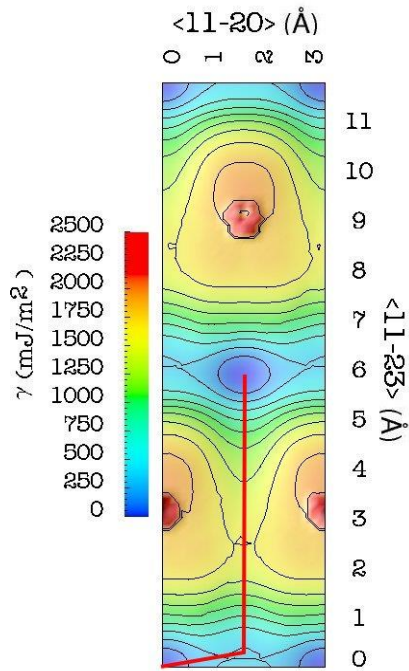


Figure 7: Zirconium. On the top left picture (a): Map of the stacking fault energy ( $\gamma$ ) in the (11-20) plan obtained by MD. On the bottom left picture (c): Map of stacking fault energy ( $\gamma$ ) in the (11-20) plan obtained by *ab initio*. On the top right (b): graphic of energetic way following the “c” direction obtained by MD. On the bottom right (d): graphic of energetic way following the “c” direction obtained by *ab initio*. The red lines represent the indirect paths.

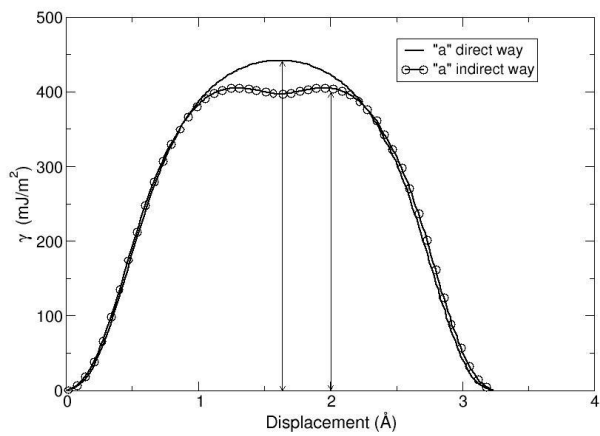
Zr

Pyramidal 1

a)



b)



c)

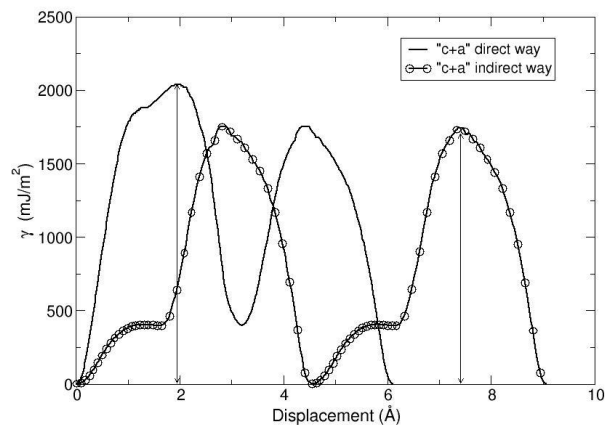
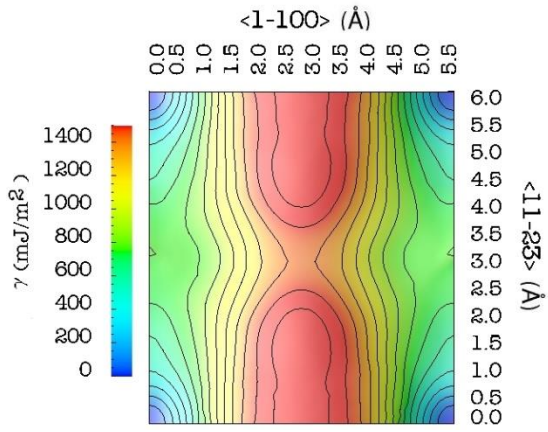


Figure 8: Zirconium. On the top left picture (a): Map of the stacking fault energy ( $\gamma$ ) in the  $(11-20)$  plan obtained by MD. On the bottom left picture (c): graphic of energetic way following the "a" direction obtained by MD. On the bottom right (d): graphic of energetic way following the "c+a" direction obtained by *ab initio*.

Zr

Pyramidal 2

a)



b)

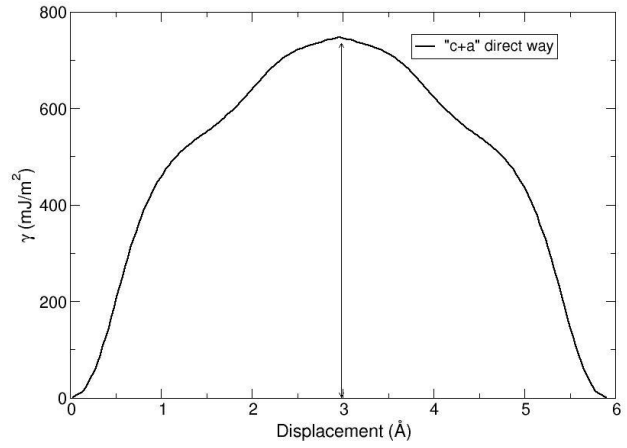


Figure 9: Zirconium. On the left picture (a): Map of the stacking fault energy ( $\gamma$ ) in the (11-20) plan obtained by MD. On the right (b): graphic of energetic way following the "c+a" direction obtained by MD.

Ti

Basal

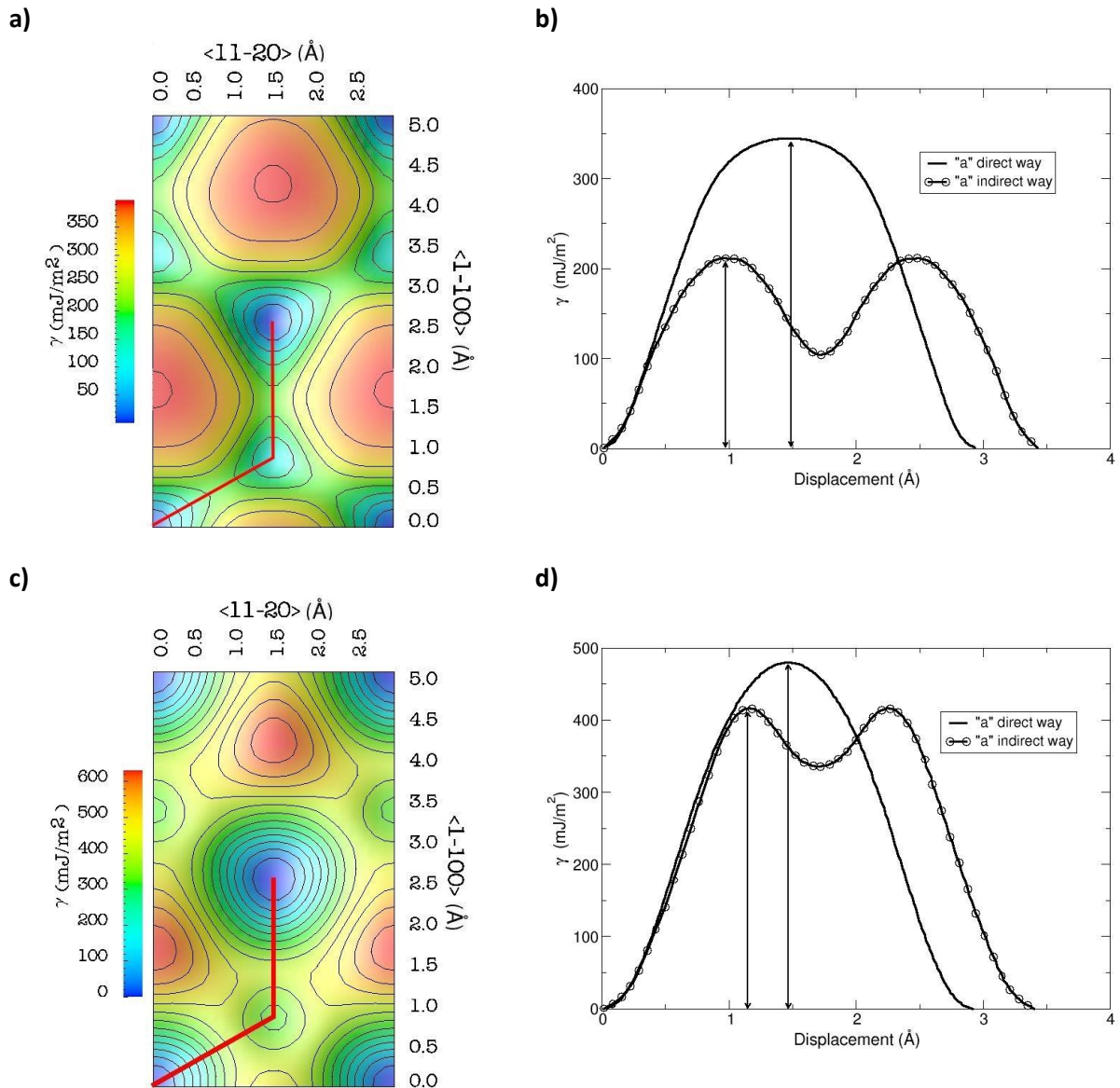


Figure 10: Titanium. On the top left picture (a) : Map of the stacking fault energy ( $\gamma$ ) in the (0001) plan obtained by MD. On the bottom left picture (c): Map of stacking fault energy ( $\gamma$ ) in the (0001) plan obtained by *ab initio*. On the top right (b): graphic of energetic way following the "a" direction obtained by MD. On the bottom right (d): graphic of energetic way following the "a" direction obtained by *ab initio*. The red lines represent the indirect paths.

i

### Prismatique

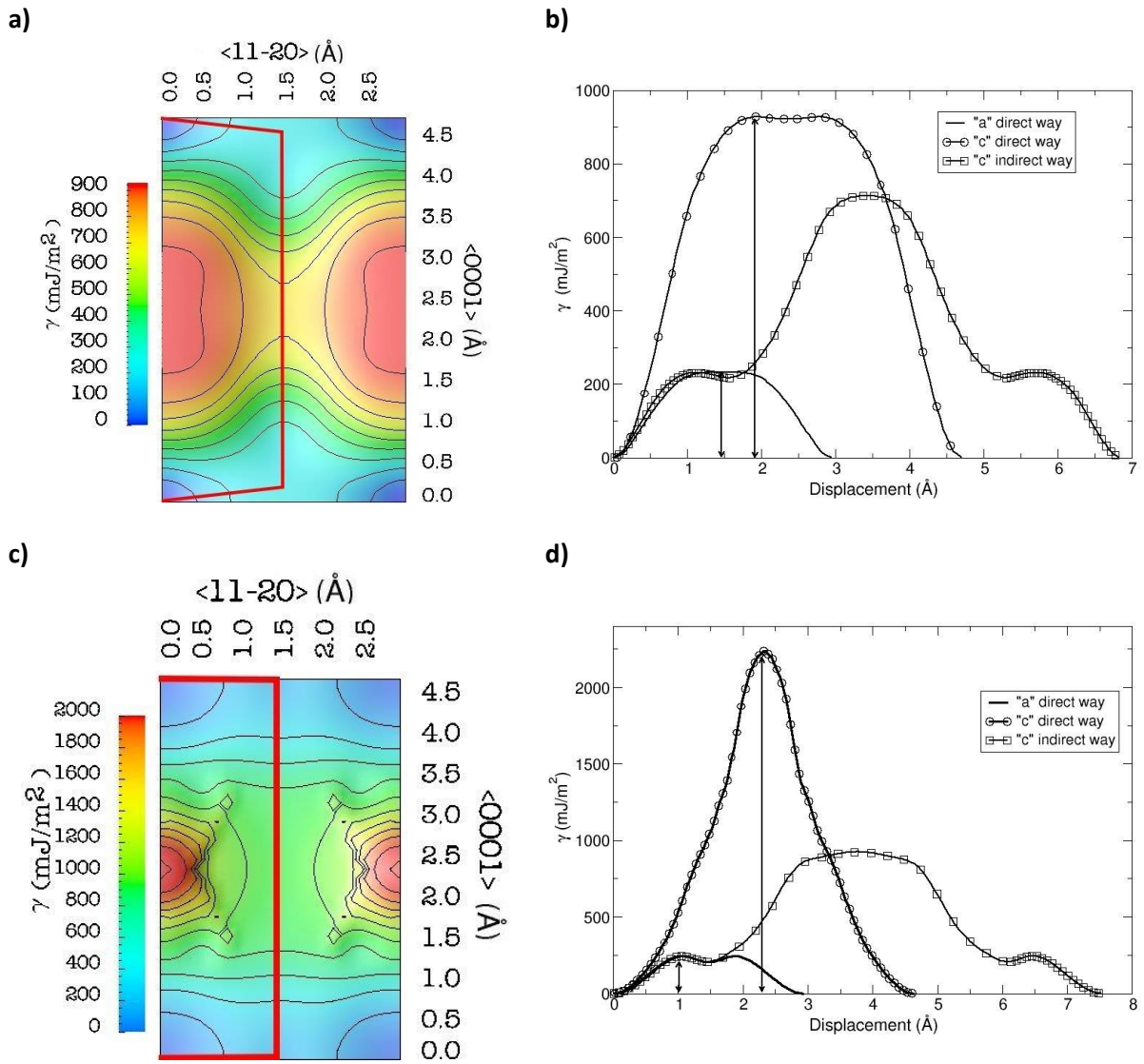


Figure 11: Titanium. On the top left picture (a) : Map of the stacking fault energy ( $\gamma$ ) in the (10-10) plan obtained by MD. On the bottom left picture (c) : Map of stacking fault energy ( $\gamma$ ) in the (10-10) plan obtained by *ab initio*. On the top right (b): graphic of energetic way following the "a" and "c" directions obtained by MD. On the bottom right (d): graphic of energetic way following the "a" and "c" directions obtained by *ab initio*. The red lines represent the indirect paths.

Ti

Prismatique2

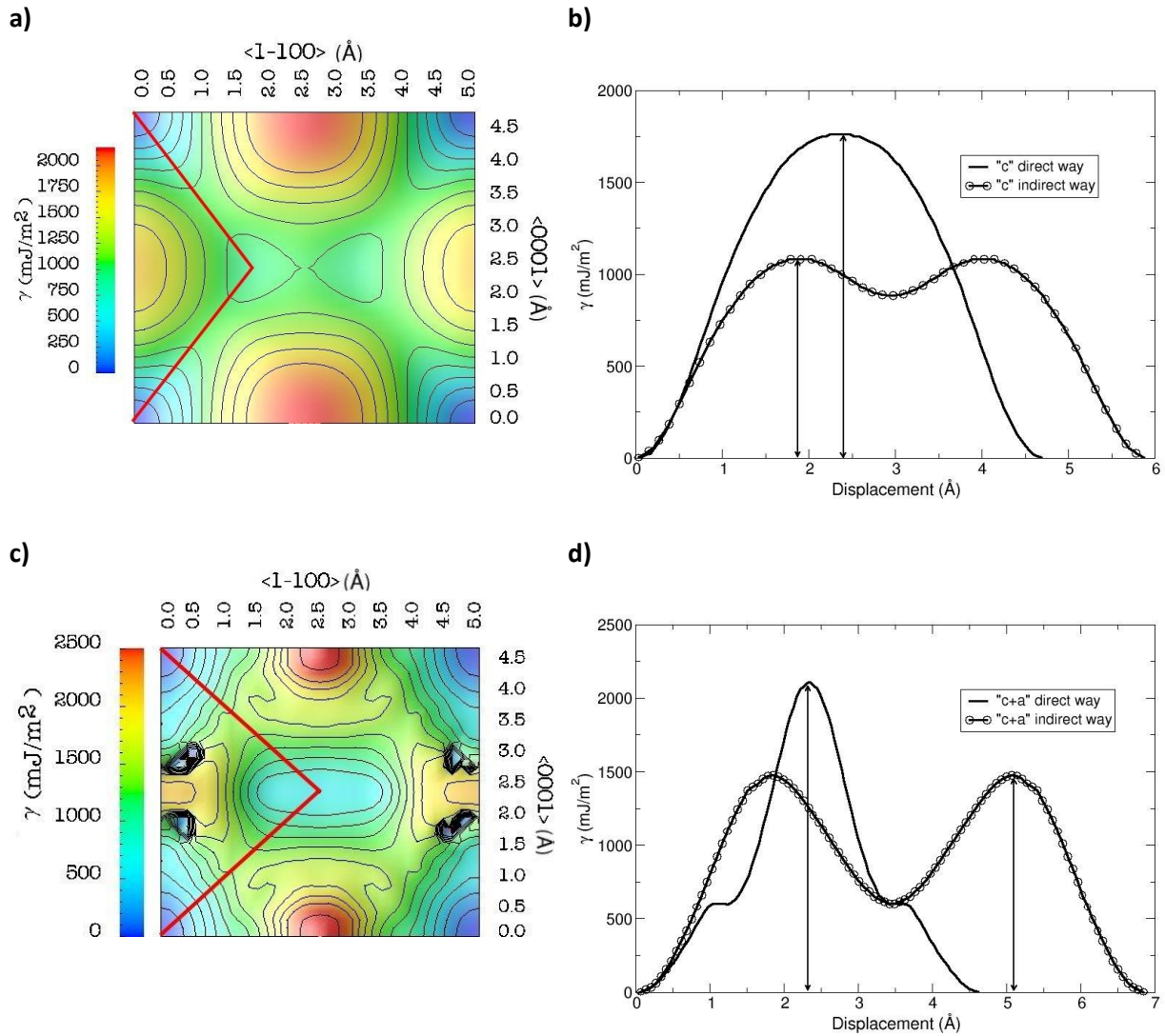
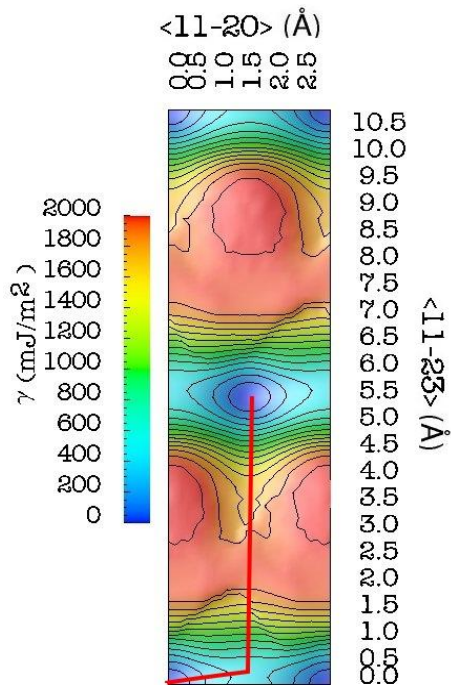


Figure 12: Zirconium. On the top left picture (a): Map of the stacking fault energy ( $\gamma$ ) in the (11-20) plan obtained by MD. On the bottom left picture (c): Map of stacking fault energy ( $\gamma$ ) in the (11-20) plan obtained by *ab initio*. On the top right (b): graphic of energetic way following the "c" direction obtained by MD. On the bottom right (d): graphic of energetic way following the "c" direction obtained by *ab initio*. The red lines represent the indirect paths.

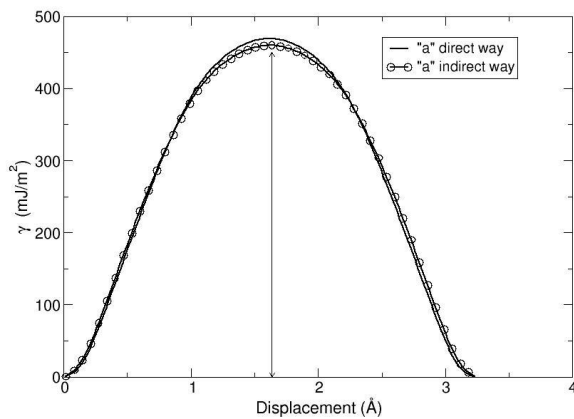
Ti

### Pyramidal 1

a)



b)



c)

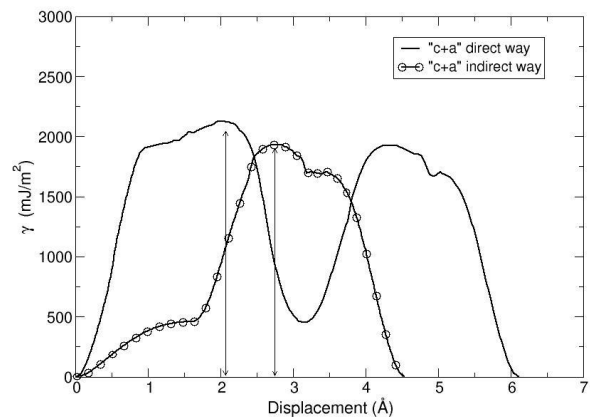
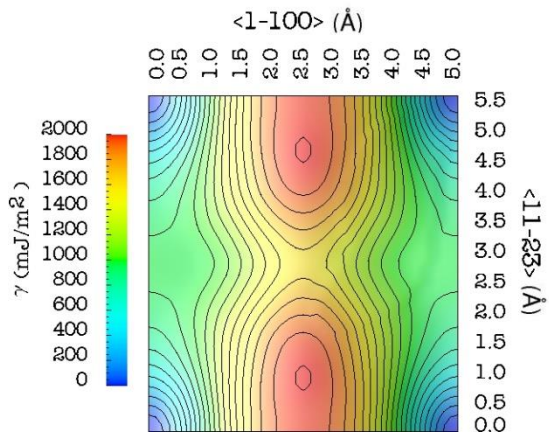


Figure 13: Titanium. On the top left picture (a): Map of the stacking fault energy ( $\gamma$ ) in the  $(11-20)$  plan obtained by MD. On the bottom left picture (c): graphic of energetic way following the "a" direction obtained by MD. On the bottom right (d): graphic of energetic way following the "c+a" direction obtained by *ab initio*. The red lines represent the indirect paths.

Ti

### Pyramidal 2

a)



b)

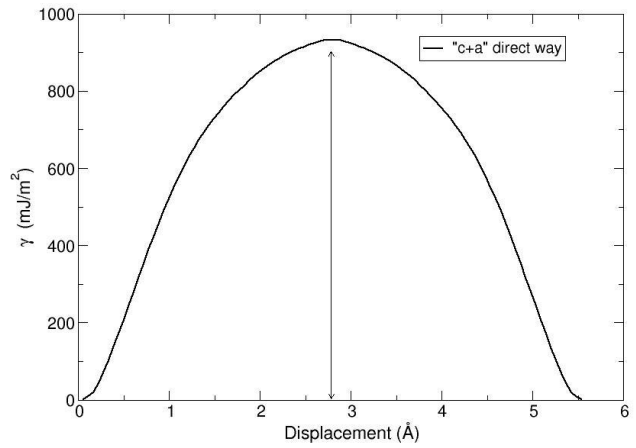


Figure 14: Titanium. On the left picture (a): Map of the stacking fault energy ( $\gamma$ ) in the  $(11-20)$  plan obtained by MD. On the right (b): graphic of energetic way following the "c+a" direction obtained by MD.

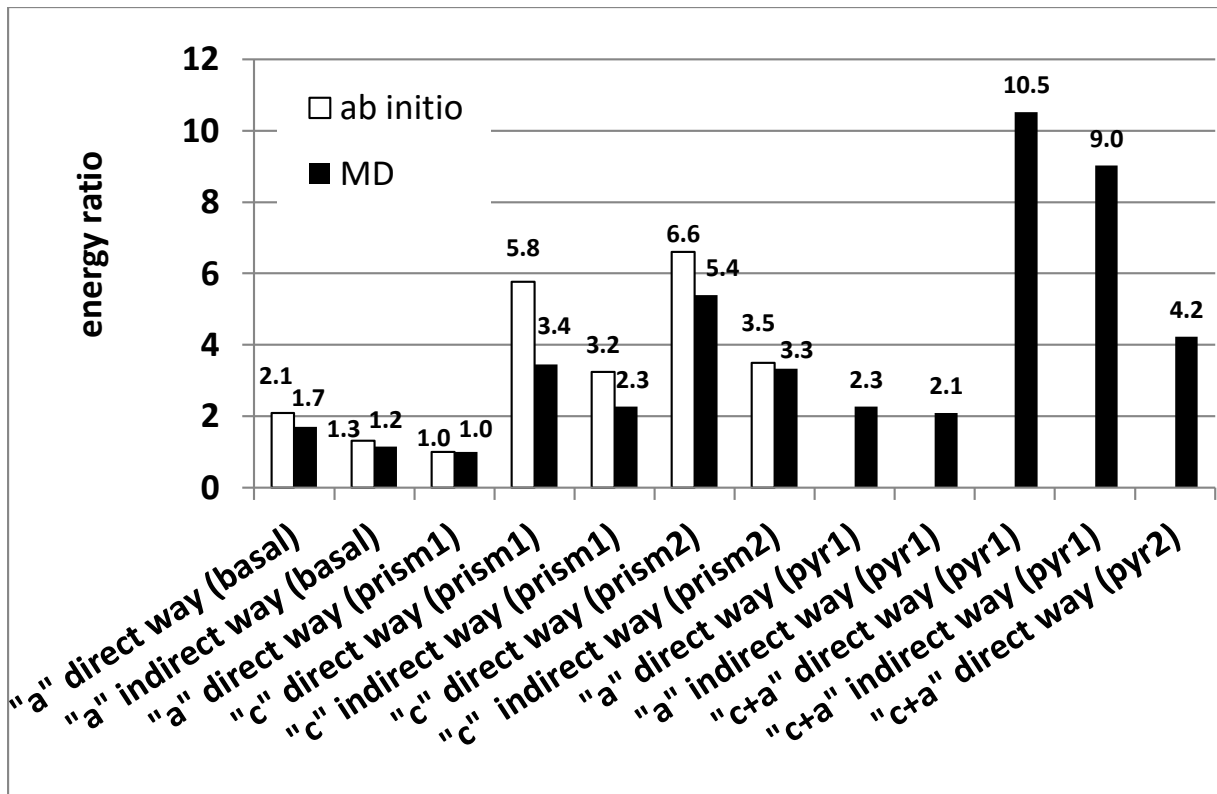


Figure 15: Zirconium normalized diagram of the maximum stacking fault energy ( $\gamma$ ) concerning three plans of glide following the "a" and "c" direction of glide obtained by MD and *ab initio* calculation.

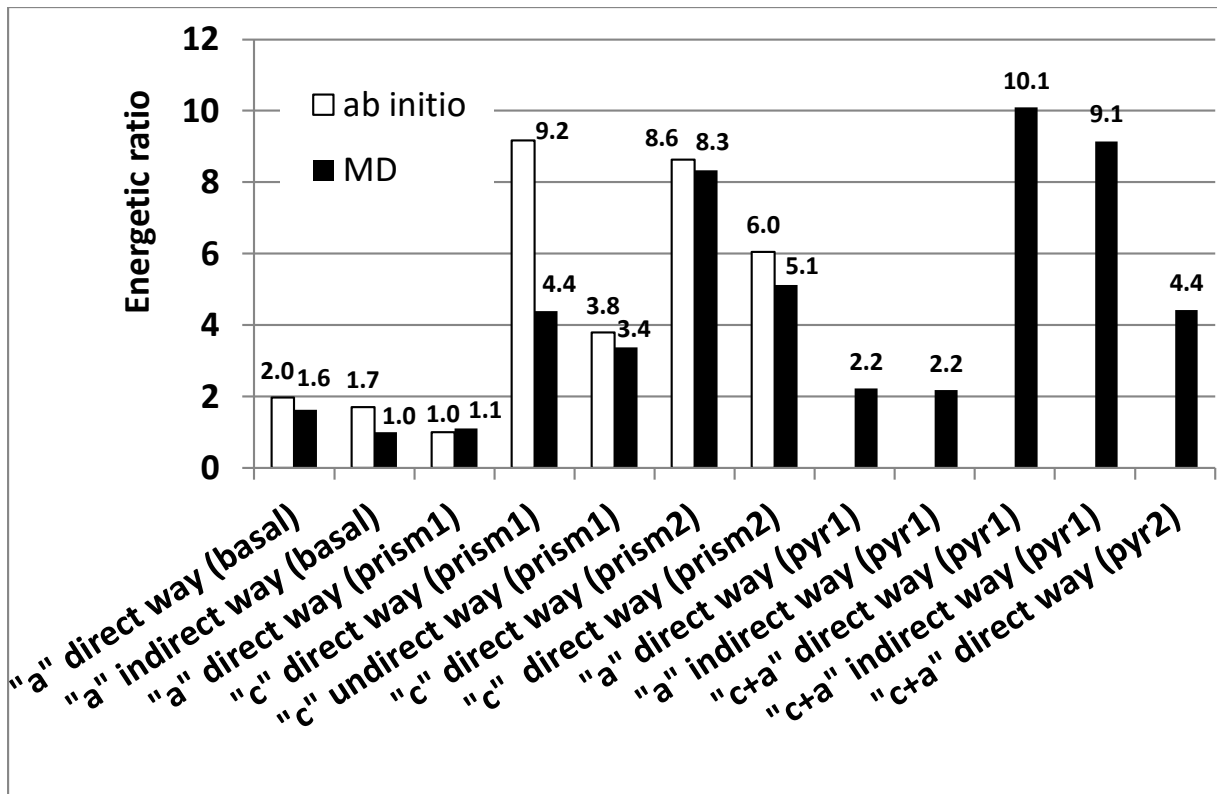


Figure 16: Titanium normalized diagram of the maximum stacking fault energy ( $\gamma$ ) concerning three plans of glide following the "a" and "c" direction of glide obtained by MD and *ab initio* calculation.

Ti

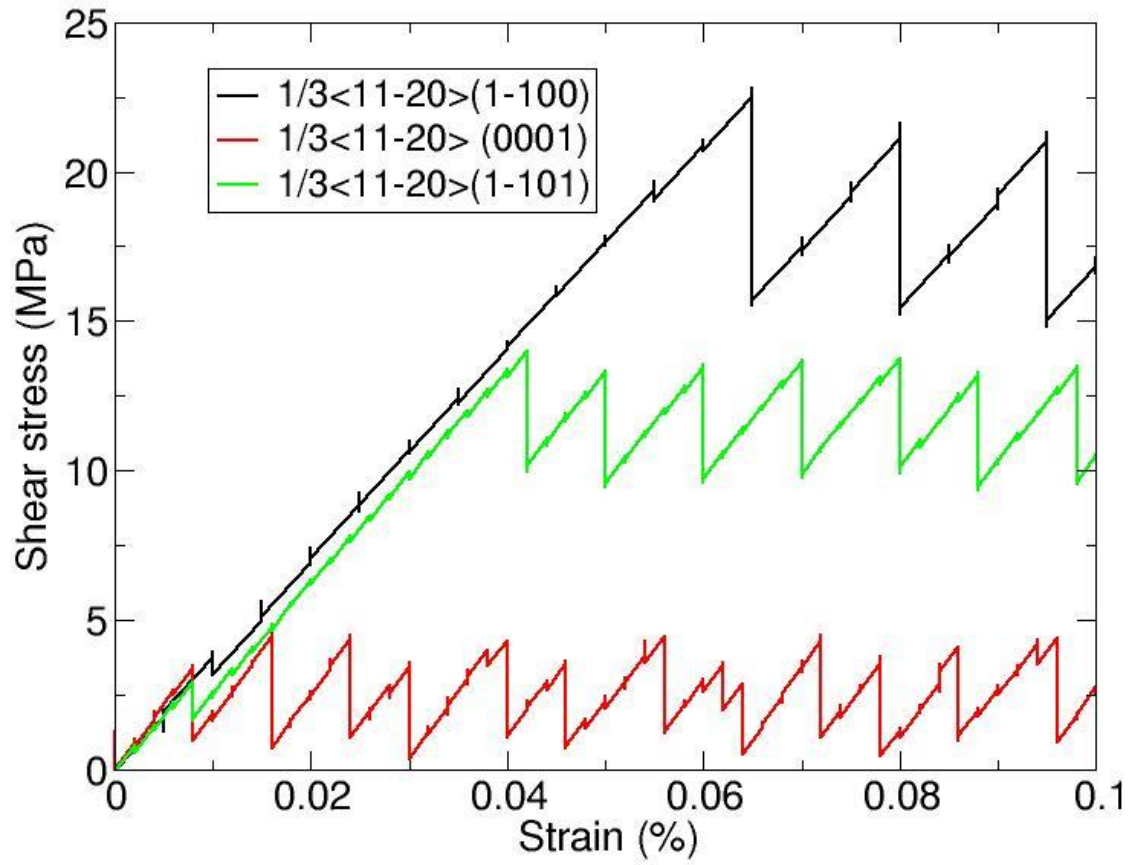


Figure 17: Resolved shear stress versus strain plots for glide of straight edge dislocation of Zr at 0 K.

Ti

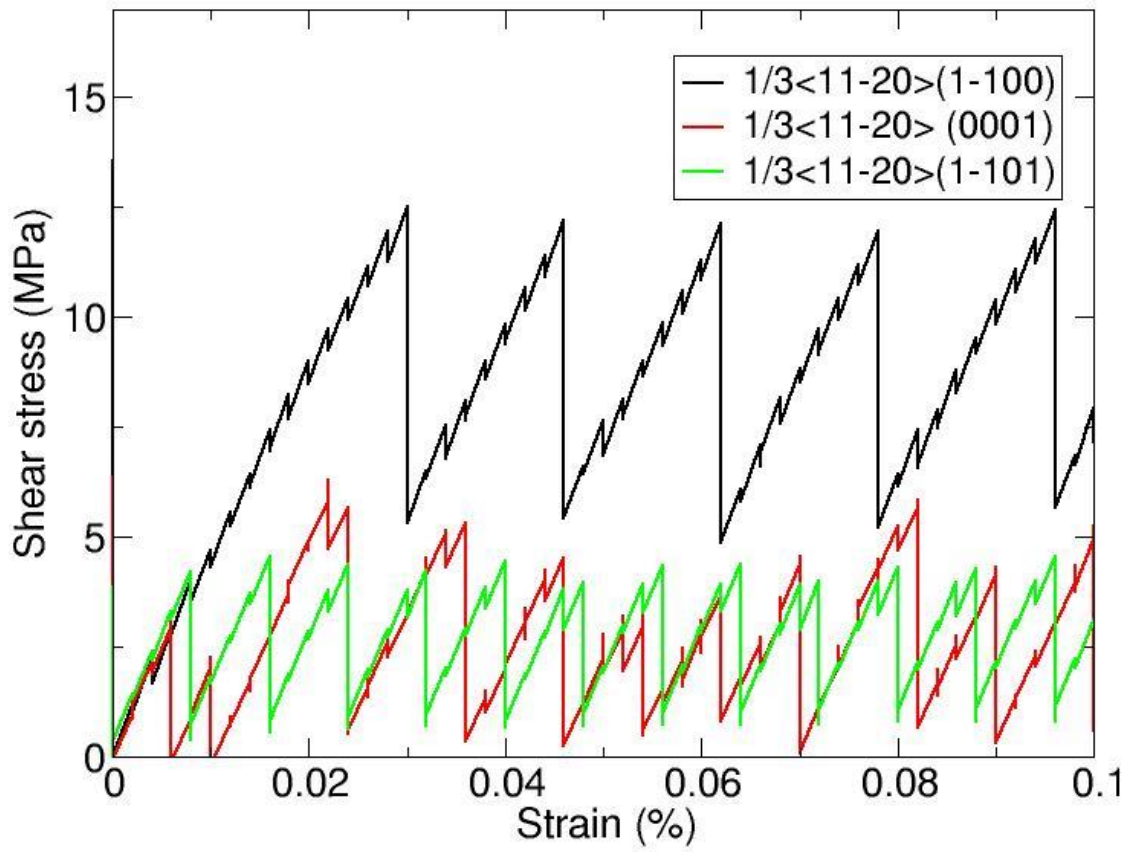


Figure 18: Resolved shear stress versus strain plots for glide of straight edge dislocation of Ti at 0 K.

## Bibliography :

- [1 ] Hutchinson W.B., Barnett M.R., Scripta Mater 63, (2010) 737
- [2] Aoki M, Nguyen-Manh D, Pettifor DG, Vitek V. Prog Mater Sci 2007 **52** 154
- [3] Proust G., Tomé C. N., Jain A and Agnew S. R., International Journal of Plasticity, 25 (2009) 86
- [4] Mendeleev MI, Ackland G. Philos Mag Lett 2007 **87** 349.
- [5] Hohenberg P., and Kohn W., Phys. Rev., 136, (1964) 864.
- [6] Kohn W., and Sham L. J., Phys. Rev., 140 (1965) 1133.
- [7] Kohn W., Phys. Rev. 133 ( 1964) 171
- [8]Hafner J., Acta Mater. **48** (2000) 71.
- [9] Kresse G. and Furthmüller J., Phys. Rev. B **54** (1996) 11169.
- [10] Kresse G. and Furthmüller J.,Comput. Mater. Sci. **6** (1996) 15.
- [11] Vanderbilt D., Phys. Rev. B **41** (1990) 7892.
- [12] Kresse G. and Hafner J., J. Phys.: Condens. Matter **6** (1996) 8245.
- [13] Perdew J. P. and Wang Y., Phys. Rev. B **45** (1991) 13244.
- [14] Monkhorst H. J. and Pack J. D., Phys. Rev. B **13** (1976) 5188.
- [15] Baskes MI, Johnson RA. Model Simul Mater Sci Eng 1994 **2** 147.
- [16] Rodney D. Acta Mater 2004 **52** 607.
- [17] Nogaret T, Robertson C, Rodney D. Philos Mag 2007 **87** 945.
- [18] Rodary E, Rodney D, Proville L, Bréchet Y, Martin G. Phys Rev B 2004 **70** 054111.
- [19] Rodney D, Martin G. Phys Rev B 2000 **61** 8714.
- [20] Osetsky YN, Bacon DJ. Model Simul Mater Sci Eng 2003 **11** 427.
- [21] Osetsky YN, Bacon DJ, de Diego N. Metall Mater Trans A 2002 **33** 777
- [22] Ackland GJ, Wooding SJ, Bacon DJ. Philos Mag A 1995 **71** 553
- [23] Johnson RA. Philos Mag A 1991 **63** 865.
- [24] Igarashi M, Khantha M, Vitek V. Philos Mag B 1991 **63** 603.
- [25] Ackland GJ, U. Pinsook. Phys. Rev. B 1998 **58** 11252.
- [26] Cleri F., Rosato V., Phys. Rev. B 1992 **48** 22.
- [27] Willaime F, Massobrio C. Phys Rev B 1991 **43** 11653.
- [28] Pasianot RC, Monti AM. J Nucl Mater 1999 **264** 198.
- [29] Khater H.A., Bacon D.J., Acta Materialia 58 (2010) 2978
- [30] Ackland GJ. Philos Mag A 1992 **66** 917.
- [31] Simmons G, Wang H. Single crystal elastic constants: a handbook. Cambridge, MA: MIT Press; 1971.
- [32] Domain C, Legris A. Philos Mag A 2005 **85** 569.
- [33] Vitek V. Prog Mater Sci 36 (1992)1. Hull D, Bacon DJ. Introduction to dislocations. 4th ed. Oxford: Butterworth; 2001. Hirth JP, Lothe J. Theory of dislocations. 2nd ed. New York: John Wiley; 1982.
- [34] Legrand B. Philos Mag B 49 (1984) 171
- [35]Legrand B. Influence de la structure électronique sur la facilité relative des glissements dans les métaux de structure hexagonale compacte. Thesis. Université Paris 6, 1984.
- [36 ] Hao Y., Zhu J., Zhang L., Qu J.,Ren H Solid State Sciences 12 (2010) 1473